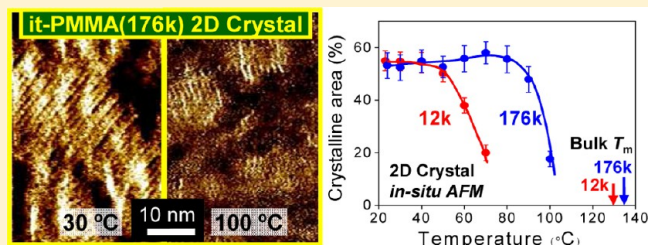


Significant Melting Point Depression of Two-Dimensional Folded-Chain Crystals of Isotactic Poly(methyl methacrylate)s Observed by High-Resolution In Situ Atomic Force Microscopy

Yuma Takanashi[§] and Jiro Kumaki*

Department of Polymer Science and Engineering, Graduate School of Science and Engineering, Yamagata University, Yonezawa, Yamagata 992-8510, Japan

ABSTRACT: The properties of polymer ultrathin films are a subject of intense study from both practical and academic viewpoints. Previously, we found that upon compression, an isotactic poly(methyl methacrylate) (it-PMMA) Langmuir monolayer crystallized to form a two-dimensional (2D) folded-chain crystal, and the molecular image of the crystal with chain folding and tie chains was clearly visualized by atomic force microscopy (AFM). In the present study, the melting behaviors of the it-PMMA 2D crystals were successfully observed *in situ* by high-temperature AFM at the molecular lever for the first time. The chain–chain distances (~ 1.2 nm) of the crystals were clearly resolved even at temperatures close to the melting temperatures (T_m) of the 2D crystals. We found that the T_m of the 2D crystals was at most 90 °C lower than the bulk T_m . The T_m depression strongly depended on the molecular weight, while the molecular weight dependence of the bulk T_m was negligible in the molecular weight regime studied. The T_m depression also depended on the substrates, a slightly larger depression being observed on a sapphire substrate compared to that on a mica. The large T_m depressions of the 2D crystals could not be explained by a simple Thomson–Gibbs argument, theoretical developments are necessary to understand the melting of the 2D crystals.



INTRODUCTION

Recently, ultrathin polymer films have received great interest from both practical and academic viewpoints. The structure and properties of the ultrathin films are expected to be significantly different from the bulk. The large surface and interfacial energies and the strong confinement into a limited thickness may greatly affect the chain conformations/packing,^{1,2} segment mobility,³⁻⁶ and thermal properties such as depression of the glass transition temperature (T_g).⁷⁻¹⁰ For a crystalline polymer, the crystal structure and morphology¹¹⁻¹⁴ are greatly affected, and the crystalline ratio and crystallization rate are suppressed in thin films.¹⁵⁻¹⁹

In spite of large numbers of reports of T_g depression in amorphous ultrathin films, reports of melting temperature (T_m) depression for crystalline films are still limited.^{13,14,19} Rafailovich and co-workers studied the T_m depression of thin polyethylene (PE) films spin-cast on various substrates (silicon, aluminum, and polyimide) with a film thickness down to 15 nm. They measured the T_m by shear modulus force microscopy, and found large T_m depression up to 38 °C at the minimum film thickness of 15 nm.^{13,14} The T_m depression depended also on the substrate identity. They pointed out that the T_m depression was slightly larger than that expected from the finite size of the crystals, then they assumed that the additional T_m depression effect was caused by substrate/PE film interactions, which also explained the T_m dependence on the nature of the substrates. This result showed a large T_m depression depending on the film thickness and the substrates;

however, the crystallized PE cast film they studied possessed complicated crystalline morphologies; the main crystalline structure changed from a spherulitic in thick films to an axialitic structure in thinner films, and from an edge-on to flat-on lamellar orientation with decreasing film thickness. A more clear result requires the use of a well-defined thin crystalline film, and also measurement of the T_m depression for much thinner region ($\ll 15$ nm) should be explored.

Previously, we studied isotactic poly(methyl methacrylate) (it-PMMA) Langmuir monolayer deposited on mica by atomic force microscopy (AFM), and found upon compression that the it-PMMA monolayer crystallized to form two-dimensional (2D) folded-chain crystals.²⁰ High-resolution AFM successfully visualized the chain packing in the folded-chain crystal with a resolution of the chain–chain distance of about 1.2 nm, and also chain folding and tie chains were visualized at the molecular level for the first time. This was a truly 2D crystal with a thickness of only a single crystalline plane and was well-aligned on the substrate as an edge-on crystal and, therefore, we think, it is an ideal model to study the physical properties of 2D crystals. In the present work, we tried to study the melting behavior of the it-PMMA 2D crystals. Since the 2D crystals are very thin, conventional measurements such as X-ray diffraction, and thermal measurements do not work well due to the limited

Received: February 4, 2013

Revised: April 5, 2013

Published: April 10, 2013

amount of the materials, hence, we tried to observe the melting behavior directly by AFM. Recently, as mentioned, by using polymer monolayers prepared by the LB technique or by spin-casting, polymer chain images with a resolution close to, or slightly better than, 1 nm were routinely attained by conventional tapping-mode AFM.^{20–31} Also, a high-resolution image of a polyethylene crystal was successfully obtained by torsional tapping-mode AFM using a T-shaped cantilever with a ultrasharp carbon whisker tip.³² Further, high-temperature AFM, AFM using a sample heating stage, enabled us to follow the crystallization/melting kinetics *in situ* at a high temperature,^{33–42} but at present the resolution at high temperature limited observations to individual lamella and visualization of individual chains inside the crystals during crystallization/melting was not attained.

In the present work, we studied the melting behavior of the 2D folded-chain crystals of it-PMMA mainly by high-temperature tapping-mode AFM, and successfully visualized it *in situ* at the molecular level, and then determined the 2D melting temperatures. The results showed extremely large T_m depressions, which also depended on the molecular weight and the substrates. The origin of the extremely large T_m depression was discussed in terms of the surface free energy and substrate effects, as well as the large molecular weight effect.

■ EXPERIMENTAL SECTION

Materials. An it-PMMA with a number average molecular weight (M_n) of 12 000, a polydispersity index (M_w/M_n) of 1.11, and a *mm* content of 97% (it-PMMA(12k)) was prepared by the isotactic-specific anionic living polymerization of MMA in toluene at $-78\text{ }^\circ\text{C}$ with *tert*-butylmagnesium bromide as an initiator.⁴³ The M_n , M_w/M_n values were measured by size exclusion chromatography (SEC) in chloroform using PMMA standards (Shodex, Tokyo, Japan) for the calibration. The tacticities were determined from the ^1H NMR signals of the α -methyl protons. An it-PMMA with a M_n of 175,700, a M_w/M_n of 1.21, and a *mm* content of 98% was purchased from Polymer Source, Inc. (Montreal, Canada). Highly purified chloroform (Infinity Pure, Wako Chemicals, Osaka, Japan) was used as the solvent for the spreading solutions without further purification. Water was purified by a Milli-Q system and used as the subphase for the LB investigations. Mica was purchased from Okenshoji Co., Ltd. (Tokyo, Japan), and sapphire (Al_2O_3) single-crystal substrate with atomically flat steps of (0001) surface⁴⁴ was purchased from Shinkosha Co., Ltd. (Yokohama, Japan). The sapphire substrate was ultrasonicated in a detergent aqueous solution for 15 min, afterward rinsed with Milli-Q water, further irradiated by a 172 nm ultraviolet light with a Xe dielectric-barrier discharge lamp (UER20-172, Ushio Inc., Japan) in air for 15 min, then rinsed with Milli-Q water before use. For the contact angle measurements, highly purified chloroform, benzene, and carbon tetrachloride (Infinity Pure, Wako Chemicals, Osaka, Japan), 1-octanol, 1-nitropropane and diiodomethane (reagent grade, Wako Chemicals, Osaka, Japan) were used without further purification.

Surface Pressure–Area (π –A) Isotherm Measurements and Langmuir–Blodgett (LB) Film Preparations for AFM. The π –A isotherms were measured as follows. An it-PMMA solution in chloroform having a concentration from 5.7×10^{-5} to 8.6×10^{-5} g/mL was spread on a water surface at $23\text{ }^\circ\text{C}$ in a commercial LB trough with an area of $60 \times 15\text{ cm}^2$, and an effective moving barrier length of 15 cm (FSD-300AS, USI, Fukuoka, Japan). The surface pressure was measured using

filter paper as the Wilhelmy plate. The π –A isotherms were measured at a constant compression rate with a moving barrier speed of 0.5 mm/s. For AFM observation, an it-PMMA monolayer was first compressed at a moving barrier speed of 0.01 mm/s to 10 mN/m (it-PMMA(176k)) and 15 mN/m (it-PMMA(12k)), then, deposited on a piece of freshly cleaved mica or cleaned sapphire plate by pulling them out of the water at a rate of 4.2 mm/min, while compressing the monolayer at the constant pressure (the vertical dipping method).

AFM Observations at Room Temperature (RT AFM).

The deposited monolayers on a mica or sapphire substrate were annealed at specific temperatures for 1 h in air by a hot stage made for optical microscopy (FP82HT/FP90, Mettler-Toledo Inc., Columbus, OH, U.S.A.), allowed to cool, then, observed by a commercial AFM (NanoScope IIIa or IV/multimode AFM unit, Bruker AXS, Santa Barbara, CA, U.S.A.) with standard silicon cantilevers (PointProbe, NCH, NanoWorld, Neuchâtel, Switzerland) in air at room temperature in the tapping mode (RT AFM). The typical settings of the AFM observations were as follows: a drive amplitude of 0.8–1.0 V, a set point of 0.68–0.92 V, and a scan rate from 1.8 to 2.2 Hz. The AFM images obtained are presented without any image processing except flattening.

In Situ AFM Observations at High Temperature (*in situ* AFM). The deposited monolayers on a mica or sapphire substrate were observed at high temperatures in air *in situ* by a high temperature AFM, Agilent 5500 AFM with a temperature control sample plate (up to a maximum of $250\text{ }^\circ\text{C}$) enclosed in an environmental chamber for stable temperature control constructed by Agilent Technologies, Inc. (Santa Clara, CA, U.S.A.). The samples were first observed at room temperature, then heated stepwise, usually at $10\text{ }^\circ\text{C}/\text{step}$, after which the temperature was allowed to stabilize until the drift became negligible, at which point the AFM observation was started, and the sequence was repeated. The overall heating rate was about $10\text{ }^\circ\text{C}/\text{h}$. For observation during a melting-and-recrystallization cycle, the heating and cooling rates were also about $10\text{ }^\circ\text{C}/\text{h}$ on average. The typical settings of the AFM observations were as follows: a drive amplitude of 1.8–2.6 V, a set point of 1.76–2.46 V, and a scan rate from 2.0 to 2.5 Hz. The AFM images obtained are presented without any image processing except flattening.

AFM Image Analysis. The length and thickness of lamella crystals were evaluated by ImageJ, public domain software from the National Institute of Health. The crystalline areas of the AFM images both in the RT AFM and *in situ* AFM measurements were evaluated by image processing software, Pico Image (Agilent Technologies, Inc., Santa Clara, CA, U.S.A.) using phase images.

Differential Scanning Calorimetry (DSC) and Wide Angle X-ray Scattering (WAXS) Measurements. The bulk melting temperatures of it-PMMA(176k) and it-PMMA(12k) were determined by DSC. Samples were solvent cast from 4-heptanone solution (5 wt %), dried in vacuo at $50\text{ }^\circ\text{C}$ for 2 h, and then annealed at $80\text{ }^\circ\text{C}$ for 72 h in vacuo.⁴⁵ The resultant crystallized it-PMMA were then investigated by DSC (Q100, TA Instruments-Waters LLC, Delaware, U.S.A.) in a nitrogen atmosphere at a heating rate of $10\text{ }^\circ\text{C}/\text{min}$. The T_m and the heat of fusion were $134.4\text{ }^\circ\text{C}$, 19.7 J/g and $130.7\text{ }^\circ\text{C}$, 34.6 J/g for it-PMMA(176k) and it-PMMA(12k), respectively. The crystalline ratio of each sample was determined by WAXS measurements using Nano-Viewer with a 2D detector, Pilatus 100K/R (Rigaku Corporation, Tokyo, Japan), and were 23.9

and 41.5% for the it-PMMA(176k) and it-PMMA(12k), respectively. The resultant heat of fusion for it-PMMA crystals were almost the same for it-PMMA(176k) and it-PMMA(12k), $\sim 1.03 \times 10^8 \text{ J/m}^3$.

Contact Angle Measurements. The surface free energy of crystallized it-PMMA, mica, and sapphire substrate was evaluated by contact angle measurement using a contact angle meter (SImage mini, Excimer Inc., Kanagawa, Japan).

An it-PMMA(176k) crystallized monolayer was deposited on a silicon substrate at 10 mN/m for 10 layers, and the contact angles of water and diiodomethane on the LB film in air were measured. Then the surface free energy of the it-PMMA crystallized monolayer was estimated according to the Owens–Wendt method.^{46,47} The polar, γ^P , disperse, γ^D , and total surface free energies, $\gamma (= \gamma^P + \gamma^D)$, of the crystalline it-PMMA were 9.2, 34.1, and 43.3, respectively, and were similar to values reported for an atactic PMMA (4.3, 35.9, and 40.2).⁴⁶

The surface energy of the high-energy surface of mica and sapphire was evaluated by measuring the contact angle of water on the substrates immersed in various organic solvents viz benzene, 1-octanol, 1-nitropropane, chloroform, and carbon tetrachloride, and the surface energy was estimated according to the method of Shultz et al.^{48,49} A freshly cleaved mica substrate and a sapphire substrate cleaned as described above were immersed in the organic solvent for 48 h prior to the measurement of the water contact angle on the substrates in the solvent. The surface energy of mica thus obtained ($\gamma^P = 84.0$, $\gamma^D = 33.3$, and $\gamma = 117.3 \text{ mJ/m}^2$) was in good agreement with the values reported previously for mica (90, 30, and 120).^{48,49} γ^P , γ^D , and γ for sapphire substrates were evaluated to be 58.4, 42.1, and 100.5 mJ/m², respectively.

RESULTS AND DISCUSSION

π -A Isotherms and 2D Folded-Chain Crystals of it-PMMA(176k) and it-PMMA(12k). Figure 1a shows π -A isotherms of it-PMMA(176K) and it-PMMA(12k). They have a plateau transition at 7 and 10 mN/m, respectively, that corresponds to their crystallization into 2D folded-chain lamella crystals.^{20,50} Figure 1b shows AFM height (upper) and high-magnification phase images (lower) of it-PMMA(176k) and it-PMMA(12k) monolayers deposited on mica at 10 and 15 mN/m, respectively, which were well-above the surface pressures for their crystallization transitions. A single monolayer was deposited on a mica substrate, and the thickness of the lamella from the substrate surface was measured to be only about 0.6 nm by AFM. The lamella of it-PMMA(176k) was relatively short and oriented randomly, whereas those of the it-PMMA(12k) were longer and well-ordered, indicating a higher probability of the crystalline nuclei formation of the high-molecular weight sample (it-PMMA(176k)). Figure 1c shows the magnified image of the lamella for an area indicated by a yellow square in Figure 1b. Helices are packed perpendicular to the long axis of the lamella with a helix–helix distance of ~ 1.23 nm (blue lines) and a helical pitch of ~ 1.05 nm (red lines), similar to that reported previously.²⁰ Kusanagi and Tadokoro studied the crystal structure of uniaxially stretched it-PMMA strands by X-ray scattering, and analyzed it to be a crystal composed of double-stranded helices.^{51,52} In their model, two 10/1 helices of it-PMMA chains (10 MMA units per turn) are intertwined to form a double helix, which packs in an orthorhombic crystal with a helix–helix distance of ~ 1.22 nm and a helical pitch of 1.05 nm. The helix–helix distance and the helical pitch were in good agreement with the values observed

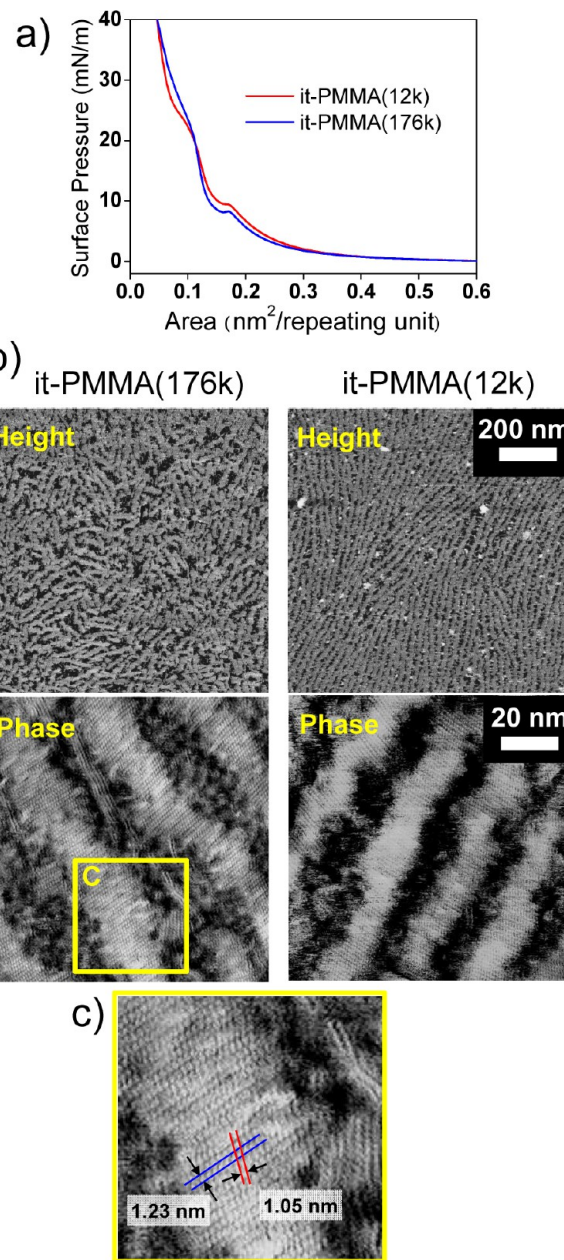


Figure 1. (a) π -A isotherms of monolayers of it-PMMA(176k) and it-PMMA(12k) on a water surface. (b) AFM height images (upper) and high-magnification phase images (lower) of monolayers of it-PMMA(176k) and it-PMMA(12k) deposited on mica at 10 and 15 mN/m, respectively. (c) Magnified AFM phase image for the area indicated by a yellow square in the bottom left of (b). The helix–helix distance (blue lines, 1.23 nm) and the helical pitch (red lines, 1.05 nm) are shown. The 2D folded-chain crystals thus obtained were subject to subsequent melting experiments.

for the Langmuir monolayers in this study, indicating the lamella are composed of the double-stranded helix of it-PMMA chains.²⁰ The average thickness of the lamella along the chain axis was 16.1 nm for it-PMMA(176k) and 13.8 nm for it-PMMA(12k). The total lengths of the double-stranded helix of it-PMMA(176k) and it-PMMA(12k) are proportional to the molecular weight and estimated to be 366 and 25 nm, respectively, assuming that a double-stranded helix is composed of two PMMA chains. Thus, the average folding numbers of the double helix in the lamella, estimated by dividing the length of

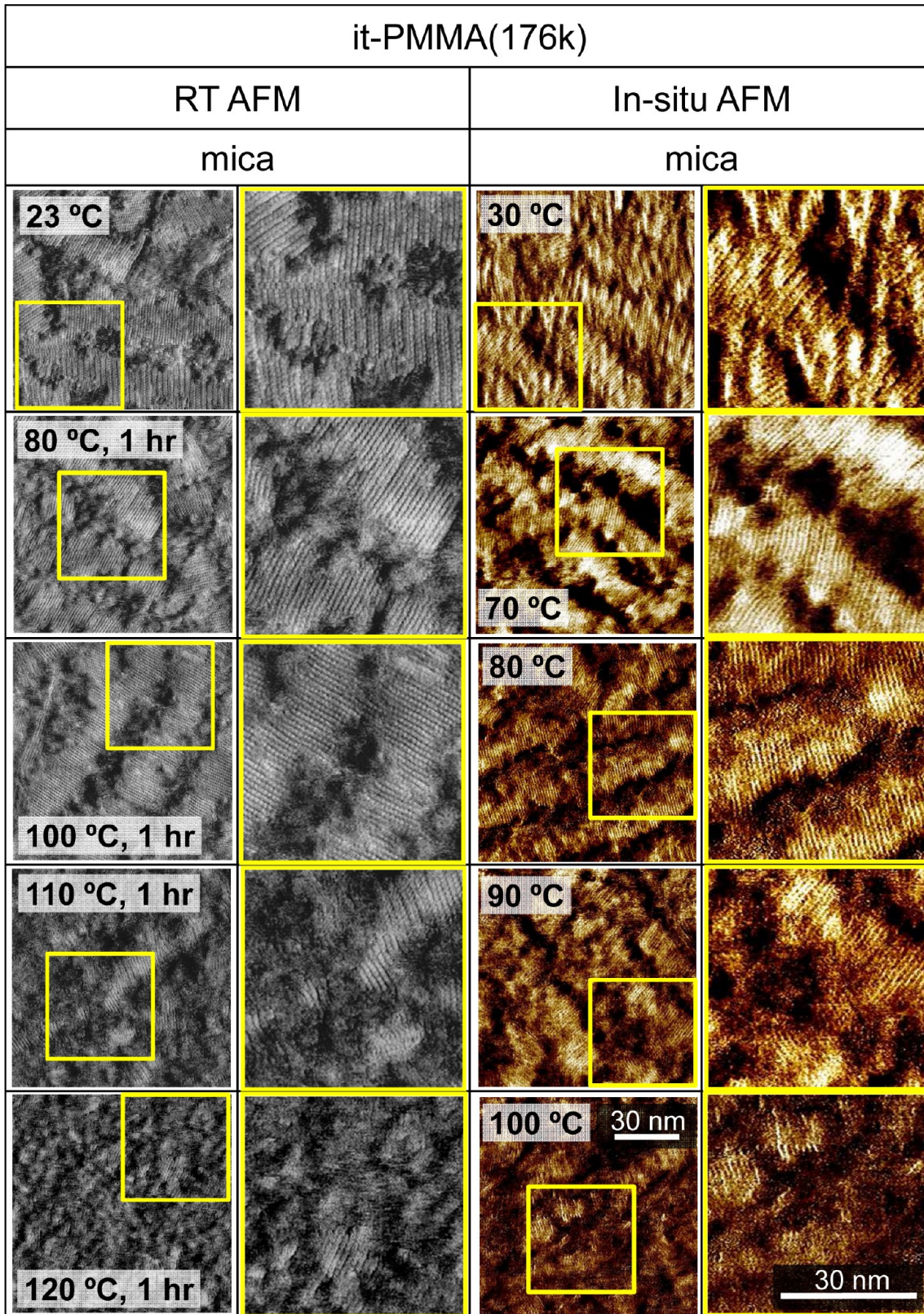


Figure 2. AFM phase images of 2D folded-chain crystals of it-PMMA(176k) deposited on mica. Gray images (left two columns): the 2D crystals were annealed at the indicated temperatures for 1 h, then observed by AFM at room temperature (RT AFM). Brown images (right two columns): the 2D crystals were heated stepwise, then observed in situ at the indicated temperatures by high-temperature AFM (in situ AFM). The images in yellow frames were magnified for the areas indicated in the images immediately to the left.

the double-stranded helix by the lamella thickness, are 23 (= 366 nm/16.1 nm) and 1.8 (= 25 nm/13.8 nm), respectively.

The folding numbers are halved, if we assume that a double-stranded helix is composed of a single it-PMMA chain. Note

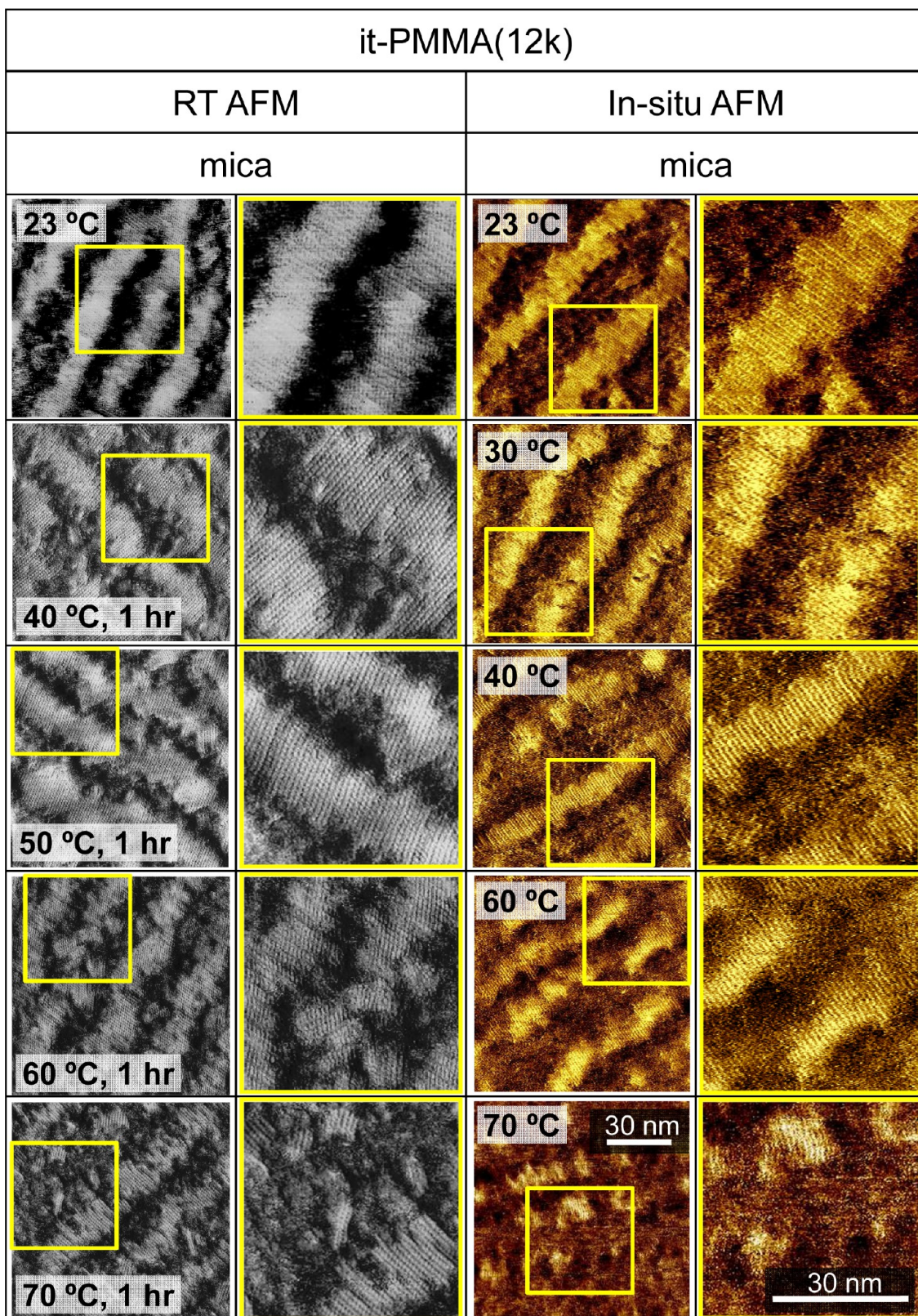


Figure 3. AFM phase images of 2D folded-chain crystals of it-PMMA(12k) deposited on mica. The gray images in left two columns and the brown images in right two columns were observed by *RT* AFM and *in situ* AFM measurements, respectively. The images in yellow frames were magnified for the areas indicated in the images immediately to the left.

that the lamellas for the both it-PMMA_s look similar, but the folding numbers of the chains are quite different. This

difference in their structures strongly affected the melting behavior of these 2D crystals as reported later.

Melting Behaviors of 2D Folded-Chain Crystals of it-PMMA Deposited on Mica. Figure 2 shows AFM phase images of 2D folded-chain crystals of it-PMMA(176k) deposited on mica during their melting. The melting behaviors were observed by two different methods. In the left two columns, 2D crystals were heated at various temperatures for 1 h, quenched to room temperature, then observed by AFM at room temperature (*RT AFM measurement*). With an increase in the temperature, the amount of the lamella decreased. A large decrease in the lamella crystal content was apparent at a temperature higher than 100 °C. On the other hand, in the right two columns, 2D crystals were observed *in situ* at various temperatures indicated in the images using the high-temperature AFM (*in situ AFM measurement*). Again, with an increase of the temperature, the amount of the lamella decreased; however, in the *in situ AFM measurement*, the lamella melted at a lower temperature than in the *RT AFM measurement*. For example, at 100 °C, most of the lamella melted in the *in situ AFM measurement*, while no significant melting was observed in the *RT AFM measurement*. This difference is presumably due to post crystallization which was unavoidable in the *RT AFM measurement*. At 100 °C, most of the lamella should melt as shown in the *in situ AFM measurement*, but the subsequent quenching to room temperature resulted in post crystallization, as shown in the *RT AFM measurement*. We emphasize that the *in situ measurement* is essential to observe the true melting behavior without post crystallization effect at the molecular level. Further, even at the temperature where most of the lamella melted, the helix–helix distances were clearly resolved. To the best of our knowledge, this is the first direct observation of melting of polymer crystals at the molecular level. The helix–helix distance was almost constant, 1.23–1.25 nm, for all the images in Figure 2, no significant broadening with heating was observed. The melting temperature, T_m , of it-PMMA(176k) in bulk was 134.4 °C as measured by DSC. In the *in situ AFM measurement*, the melting started at around 80 °C; that is, a significant melting point depression was observed for the 2D crystal. We also note that we did not find any significant roughening of the monolayers, in other words, any reconstruction of the 2D crystal to a 3D one during the experiments; this indicated that the attractive interaction between the it-PMMA and the substrate was strong enough to hold the monolayer in the 2D state, and the melting and post crystallization process basically proceeded in the 2D state.

Figure 3 shows AFM phase images of 2D folded-chain crystal of the low molecular weight it-PMMA(12k) deposited on mica. The melting seemed to start at around 50 and 40 °C for the *RT* and *in situ AFM measurements*, respectively. Again, post crystallization effect was apparent for the *RT AFM measurement*, for example, at 70 °C, most of the lamella crystals were melted in the *in situ AFM measurement*, while in the *RT AFM measurement*, significant amount of the crystals remained, probably most of which crystallized during quenching the crystals to the room temperature. Note that the melting starting at around 40 °C for it-PMMA(12k), about 40 °C lower than the melting of 2D crystal of it-PMMA(176k) in the *in situ AFM measurement*. The bulk T_m of it-PMMA(12k) measured by DSC was 130.7 °C, only slightly lower than that of it-PMMA(176k). Thus, while the molecular weight dependence of the T_m of the bulk crystals was negligible over this molecular weight range, the T_m of the 2D crystals was more significantly depressed for the lower-molecular weight crystals. The helix–helix distances of all the images in Figure 3 were 1.22–1.24 nm, almost

constant within the experimental error, and no significant broadening was observed.

In Figure 4, the lamella length, thickness, and crystalline area of 2D crystals during melting for Figures 2 and 3 are

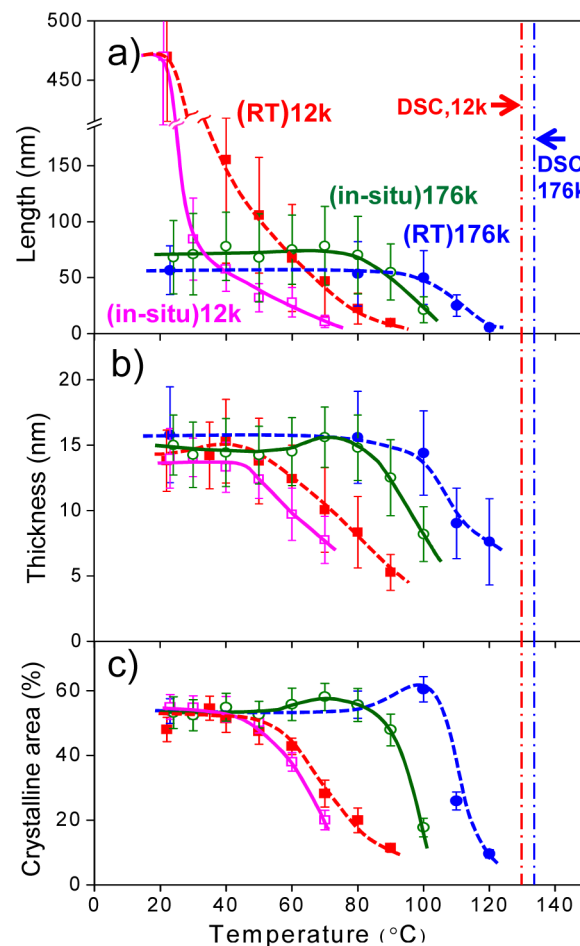


Figure 4. Lamella length (a), lamella thickness (b), and crystalline area (c) of 2D folded-chain crystals of it-PMMA(176k) and it-PMMA(12k) deposited on mica as a function of the temperature for *RT AFM* (dotted lines) and *in situ AFM* (solid lines) measurements. Melting temperature of it-PMMA bulk crystals measured by DSC are also indicated (blue dashed-dotted line: it-PMMA(176k), red dashed-dotted line: it-PMMA(12k)).

summarized. The lamella length is defined as the length of the long axis of the lamella (perpendicular to the chain axis), the thickness of lamella is the short axis of the lamella (parallel to the chain axis). The crystalline area is the area ratio occupied by lamella in AFM images and is thus considered as an index of the crystalline ratio of the 2D crystals. As mentioned, the lamella length of the original it-PMMA(12k) 2D crystals was quite high; thus, on heating, it was significantly reduced. Except for the lamella length of the it-PMMA(12k), all other values (the lamella length of it-PMMA(176k), the lamella thicknesses and crystalline areas of the it-PMMA(12k and 176k)) reduced similarly on heating. Since the surface free energy of the two sides of the lamella crystal, perpendicular (chain-folding side) and parallel to the chain axis, are expected to be very different, an anisotropic melting may be expected. But, as shown in Figure 4, the length and thickness of the lamella reduced

similarly, and so no significant anisotropy of the melting was observed.

Typically, with a rise in the temperature, the dimensional values of the lamellas were constant or slightly increased, possibly due to annealing of the crystals, and then rapidly decreased. From the inflection points for the rapid decrease, the 2D T_m was determined as shown in Table 1. The T_m values of

Table 1. Melting Temperatures of 2D Folded-Chain Crystals of it-PMMA(12k) and it-PMMA(176k) Deposited on Mica and Sapphire as Determined by RT and *in situ* AFM Observations along with Those in the Bulk

polymer/substrate	T_m by RT AFM/°C	T_m by <i>in situ</i> AFM/°C	T_m by DSC/°C
it-PMMA(12k)/mica	50	45	—
it-PMMA(12k)/sapphire	—	40	—
it-PMMA(12k)(bulk)	—	—	130.7
it-PMMA(176k)/mica	100	80	—
it-PMMA(176k)/sapphire	—	60	—
it-PMMA(176k)(bulk)	—	—	134.4

2D folded-chain crystals determined by the *in situ* AFM observation (it-PMMA(12k): 45 °C, it-PMMA(176k): 80 °C) were always lower than those observed by the RT AFM observation (it-PMMA(12k): 50 °C, it-PMMA(176k): 100 °C),

because they are free from post crystallization. Significant melting point depressions of the T_m values measured by the *in situ* AFM observation from the bulk T_m were observed (it-PMMA(12k): 86 °C, it-PMMA(176k): 54 °C). Further, the molecular weight dependence of the bulk T_m was negligible (3.7 °C), but that of the 2D crystals by the *in situ* measurement (35 °C) was significant. As mentioned above, the number of chain foldings in the 2D lamella crystals differed by more than 1 order of magnitude (it-PMMA(12k): 1.8 folds, it-PMMA(176k): 23 folds), this may explain the large molecular weight dependence of the T_m of the 2D crystals. We anticipated that the large difference in the folding number may be reflected in the melting behavior, especially on the lamella thickness distributions during the melting. Figure 5 shows the histograms of the lamella thickness distribution of 2D folded-chain crystals of it-PMMA(12k and 176k) during melting. The lamella thickness distribution was obtained by measuring the lengths of individual double stranded helices in the lamella. Although the numbers of chain foldings were very different, significant difference in the distributions of the thickness during the melting was not observed. The lamella thicknesses started reducing around the 2D T_m defined in Table 1.

Reversibility of Melting of 2D Folded-Chain Crystal of it-PMMA during a Heating–Cooling Cycle. As described above, we have evaluated T_m of the 2D folded-chain crystals by *in situ* AFM observation on heating. Skeptical readers may suspect that the melting observed here was not a true melting

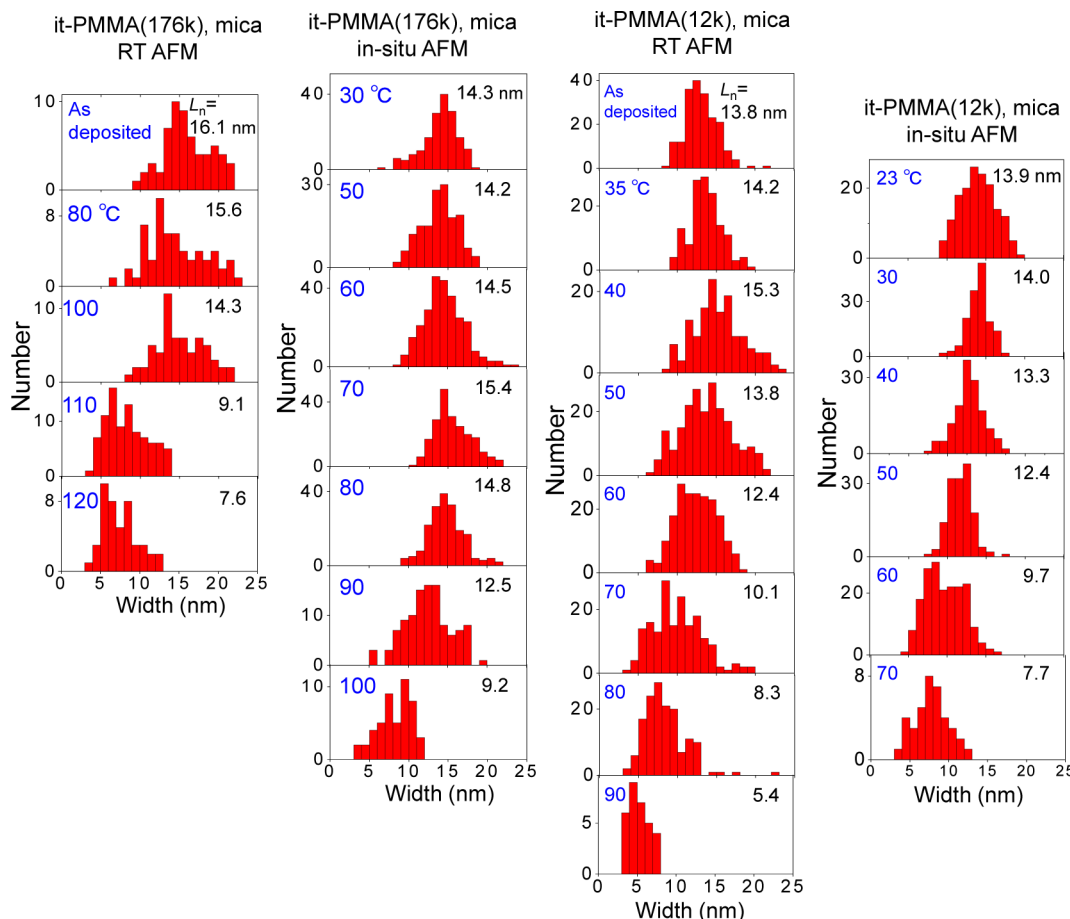


Figure 5. Histograms of lamella thickness distribution of 2D folded-chain crystals of it-PMMA(176k) and it-PMMA(12k), during RT AFM and *in situ* AFM measurements. The number-average lamella thickness, L_n , was indicated.

transition but breaking of the lamella crystals by scanning. Hence, we must consider possible tip effect in AFM observations, especially in high-resolution imaging where the tip effect might be larger. As shown in the Experimental Section, our conditions for AFM observation were selected to minimize the tip force to be as low as possible, while keeping stable imaging. During the *in situ* AFM observation on heating, we often confirmed that the melting behavior in a scanning area was the same as that outside the scanning area by reducing the magnification or shifting the scan area.

In this section, we confirm the reversibility of the melting of the 2D folded-chain crystals. Figure 6a shows high magnification AFM phase images of a 2D folded-chain crystal of it-PMMA(12k) on mica observed *in situ* during a heating-and-cooling cycle. The heating and cooling rates were about $10\text{ }^{\circ}\text{C}/\text{h}$ as mentioned in the Experimental Section. The 2D crystals were first heated stepwise up to $70\text{ }^{\circ}\text{C}$, where about two-third of the lamellas melted, and the thickness of the lamella reduced, but during the subsequent cooling, the lamella crystals almost perfectly recovered. Figure 6b shows the crystalline area and the thickness of the 2D lamella crystals during the heating-and-cooling cycle. Both area and thickness values during the melting and recrystallizing traced almost the same line, indicating that the melting was reversible. Therefore, the melting behaviors observed here were close to those of thermodynamical transition, and not breaking of the lamella due to the effects of scanning.

The reversibility should depend on the heating and cooling rate, and the rate dependence may provide important information about their kinetics. However, we did not study this, because the sufficiently slow heating and cooling rate was necessary to avoid the drift during the high-magnification AFM observations in this study.

Melting Behaviors of 2D Folded-Chain Crystals of it-PMMA Deposited on Sapphire. As mentioned above, we observed the melting behaviors of it-PMMA 2D folded-chain crystals on mica by *in situ* AFM observation and found that the T_m of the 2D crystals was depressed by 54 to $86\text{ }^{\circ}\text{C}$ from those in the bulk. This large T_m depression should mainly be attributed to the significant surface free energy of these ultrathin monolayers, but we also need to consider the monolayers–substrate interactions which are strong enough to hold the monolayers in the 2D states. Thus, in this section, in order to evaluate the effect of the substrate interaction on the T_m depression, we evaluated the behavior of monolayers deposited on a different substrate.

In order to observe the 2D crystals by AFM at the molecular level, the substrate should be molecularly flat and have sufficient affinity for the monolayer to keep it stable enough to withstand AFM observation. Highly oriented pyrolytic graphite, HOPG, often used in scanning probe microscopy, had not sufficient affinity for the it-PMMA monolayer, and could not be used. In this work, we used a sapphire substrate ($\alpha\text{-Al}_2\text{O}_3$) instead of mica, and the 2D T_m was evaluated. The sapphire substrate used was a mirror-polished single crystal with a (0001) plane, subjected to thermal annealing at temperature between 1000 and $1400\text{ }^{\circ}\text{C}$ and, as a result, had an atomically flat surface.⁴⁴ Undoubtedly, the substrates have terraces due to unavoidable small mis-orientations of the surface; however, in our high-magnification AFM observations, the sapphire terraces were broad enough to observe 2D crystals on a single terrace.

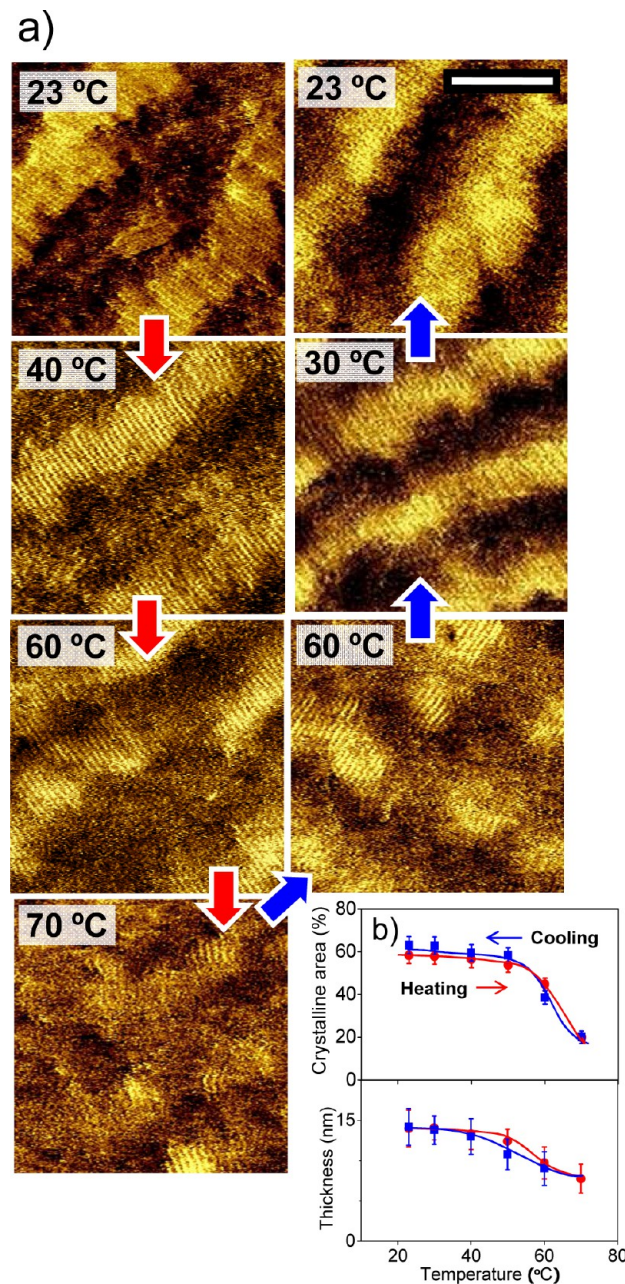


Figure 6. (a) AFM phase images of 2D folded-chain crystals of it-PMMA(12k) on mica observed *in situ* by high-temperature AFM (*in situ* AFM) during a heating-and-cooling cycle. The crystals were first heated from 23 to $70\text{ }^{\circ}\text{C}$ in a stepwise manner, then cooled in steps to $23\text{ }^{\circ}\text{C}$. Scale bar = 20 nm . (B) The crystalline area and lamella thickness of the 2D crystal during the heating and cooling cycle. Note that the it-PMMA monolayer was reversibly recrystallized during the cooling process.

The surface free energy was evaluated by contact angle measurements, and was 100.5 mJ/m^2 for sapphire and 119.1 mJ/m^2 for mica. Since the surface free energy of the crystallized it-PMMA was evaluated as 43.4 mJ/m^2 , a slightly better affinity of the PMMA crystal to the sapphire than to the mica was expected.

Figure 7 shows AFM phase images of 2D crystals of it-PMMA(176k) and it-PMMA(12k) on sapphire observed *in situ* by the high-temperature AFM. The 2D folded-chain crystals were visible also on the sapphire substrate with the clear

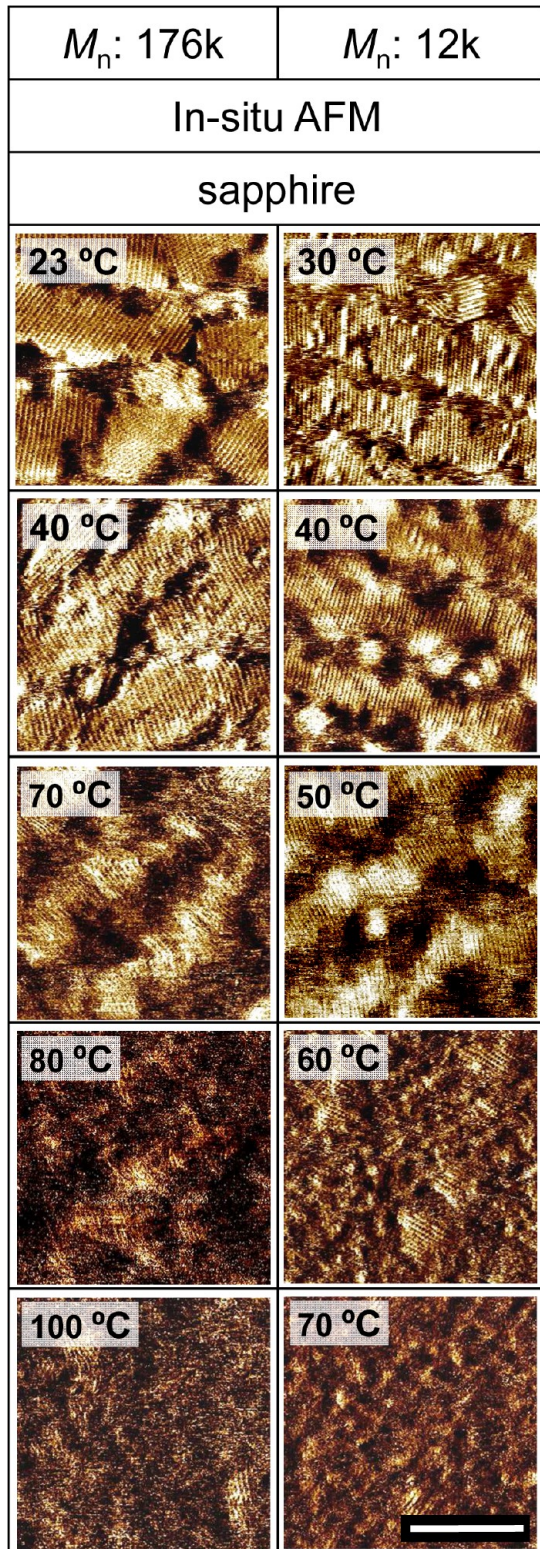


Figure 7. (A) AFM phase images of 2D crystals of it-PMMA(176k) and it-PMMA(12k) deposited on sapphire observed in situ by high-temperature AFM (*in situ* AFM). Scale bar = 30 nm.

resolution of the helix–helix distances. In comparison with the *in situ* melting behaviors of it-PMMA 2D crystals deposited on mica (Figures 2 and 3), those deposited on sapphire were found to be melted at slightly lower temperatures. Thus, it-PMMA(176k) crystals on sapphire were significantly melted at

70 °C and only a small amount of the crystals remained at 80 °C. In contrast, the same crystals on mica still mostly remained at 80 °C in the same type of *in situ* AFM observation (Figure 2, right two columns), indicating that the T_m of the it-PMMA(176k) was more depressed on the sapphire. Similar behavior was observed for the it-PMMA(12k) crystals. The 2D it-PMMA(12k) crystals on sapphire significantly melted at 60 °C, while, on the other hand, a significant amount of the crystals on mica still remained at the same temperature (Figure 3, right two columns), again indicating a large T_m depression for the crystal on sapphire. The lamella thickness distributions during the melting are summarized in Figure 8.

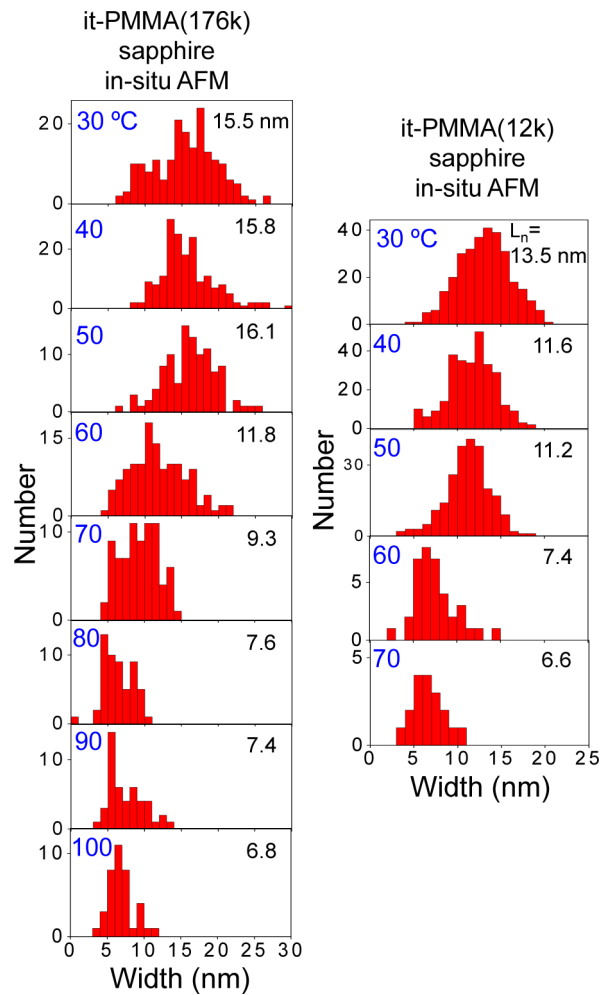


Figure 8. (A) Histograms of lamella thickness distribution of 2D folded-chain crystals of it-PMMA(176k) and it-PMMA(12k) on sapphire during *in situ* AFM measurements. The number-average lamella thickness, L_n , is indicated.

Figure 9 shows the lamella thicknesses and the crystalline areas of it-PMMA(176k and 12k) crystals on both mica and sapphire substrates observed by *in situ* AFM. For both it-PMMA(176k and 12k), the crystals on sapphire (dark blue (176k) and orange (12k) dotted lines) melted at lower temperature than those on mica (green (176k) and pink (12k) solid lines). The 2D T_m thus determined are summarized in Table 1 and show how, as mentioned earlier, the T_m of 2D crystals is affected by the substrates.

Discussion of the Origin of the Large Melting Point Depression of 2D Folded-Chain Crystals. As detailed

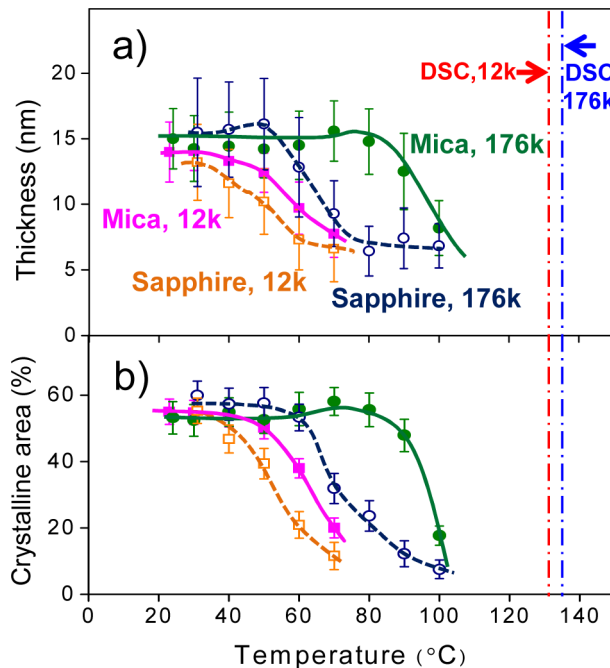


Figure 9. Lamella thickness (a) and crystalline area (b) of 2D folded-chain crystals of it-PMMA(176k) and it-PMMA(12k) deposited on mica (green solid line: it-PMMA(176k), pink solid line: it-PMMA(12k)) and sapphire (dark blue dotted line: it-PMMA(176k), orange dotted line: it-PMMA(12k)) during *in situ* AFM measurement. Melting temperature of it-PMMA bulk crystals determined by DSC are also indicated (blue dashed-dotted line: it-PMMA(176k), red dashed-dotted line: it-PMMA(12k)).

above, a significant melting point depression of the 2D folded-chain crystals of the it-PMMAAs ranging up to 90.7 °C was observed by *in situ* AFM observation. The melting point depression was more significant for the lower-molecular weight sample (12k) than for the higher molecular weight (176k), and slightly larger for a sapphire substrate than for a mica surface, as summarized in Table 1. In this section, we try to roughly evaluate the T_m depression of the 2D crystals on the basis of simple calculations.

The melting point of a finite size crystal can be expressed in a manner similar to that of the Thompson–Gibbs equation as below,^{13,14}

$$T_m = T_m^0 \left(1 - \frac{2\gamma_e}{l\Delta H_0} - \frac{2\gamma_i}{x\Delta H_0} \right) \quad (1)$$

where T_m^0 is the melting point of the ideal infinitely large crystal; l and x are the lamella thickness along the chain axis and the crystalline thickness from the substrate surface as defined in Figure 10, and γ_e and γ_i are the surface free energy of a crystal plane perpendicular (chain-folded plane) and parallel to the chain axis, respectively. ΔH_0 is the enthalpy of melting per unit volume. Without the third term on the right side, eq 1 is the well-known Thompson–Gibbs equation which shows the T_m dependence on the lamella thickness, l . The third term was added to include a contribution of the surface free energy for the ultrathin edge-on lamellar crystal.^{13,14} Since the lamella length, y , was much larger than l and x as $y \gg l > x$, thus, a corresponding term for y was neglected in eq 1.

We take $l = 16$ nm and $x = 1.2$ nm and use $\Delta H_0 = 1.03 \times 10^8$ J/m³ which is based on the DSC/WAXS measurements of the

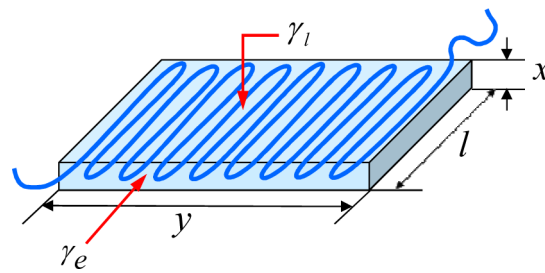


Figure 10. Schematic representation of a 2D folded-chain crystal. l : lamella thickness, y : lamella length, x : crystalline thickness from the substrate. γ_e and γ_i : surface free energy of a crystal plane perpendicular (chain-folded plane) and parallel to the chain axis, respectively.

it-PMMA bulk crystal (see the Experimental Section). γ_i is assumed to 43 mJ/m² from the surface free energy measured for the it-PMMA crystalline LB film with a crystalline area ratio of ~55% (Experimental Section). Since this value is similar to that reported for an amorphous PMMA, 40.2 mJ/m²,⁴⁶ the crystalline surface free energy is assumed to be little different from that of the amorphous polymer. We assumed $\gamma_e = 100$ mJ/m², and $T_m^0 = 463$ K, thereby obtaining a melting temperature depression that should be about 378 °C ($T_m = -188$ °C), an extremely large value in comparison to the observed values in Table 1. Since the exact γ_e , T_m^0 values for the it-PMMA crystal were not reported, we assumed the above values for the estimation. However, the contributions of γ_e and T_m^0 were limited; the main contribution was from the third term in eq 1 because of the extremely small x value (1.2 nm) in this calculation. Thus, the estimated extremely large T_m depression is at least qualitatively valid.

Equation 1 was derived by accounting for contributions of the surface free energy due to the finite size of the crystal. In the real 2D state, we may consider additional effects from the PMMA/substrate interface energy, $\gamma_{\text{PMMA/substrate}}$. Then we may rewrite eq 1 as follows.

$$T_m = T_m^0 \left(1 - \frac{2\gamma_e}{l\Delta H_0} - \frac{\gamma_i}{x\Delta H_0} - \frac{\gamma_{\text{PMMA/substrate}}}{x\Delta H_0} \right) \quad (2)$$

The interface free energy can be derived by eq 3.⁴⁶

$$\begin{aligned} \gamma_{\text{PMMA/substrate}} = & \gamma_{\text{PMMA}} + \gamma_{\text{substrate}} - 2(\gamma_{\text{PMMA}}^d \times \gamma_{\text{substrate}}^d)^{1/2} \\ & - 2(\gamma_{\text{PMMA}}^p \times \gamma_{\text{substrate}}^p)^{1/2} \end{aligned} \quad (3)$$

Using the observed γ_{PMMA} , γ_{mica} , and γ_{sapphire} (see Experimental Section), we calculated $\gamma_{\text{PMMA/mica}} = 37.7$ mJ/m² and $\gamma_{\text{PMMA/sapphire}} = 21.5$ mJ/m². Then, using the same parameters as above, we obtained the T_m of the it-PMMA 2D crystal on mica (−168.5 °C, $\Delta T_m = -359$ °C) and on sapphire (−107.8 °C, $\Delta T_m = -298$ °C). These new T_m values were slightly higher than those estimated from eq 1 but are still extremely low compared to those observed by AFM (Table 1); in addition, the slightly larger T_m depression on sapphire than on mica was not explained by eqs 2 and 3. The estimations using both eqs 1 and 2 failed to adequately explain the T_m depression of the it-PMMA 2D crystals.

As a next step to resolve this issue, we should reconsider the role of T_m^0 . The melting temperature is expressed as $T_m^0 = (\Delta H_0)/(\Delta S_0)$, since melting occurs when $\Delta G = \Delta H_0 - T\Delta S_0 = 0$, where ΔG_0 , ΔH_0 , and ΔS_0 are respectively the free energy, enthalpy, and entropy change of melting per unit volume.¹⁴ In the 2D crystal, ΔH_0 and ΔS_0 may be significantly different from

the bulk, and as a result, T_m^0 should also be different. The chains in a 3D crystal are surrounded by the other chains, whereas the chains in the 2D crystal are deposited on a substrate and the other side of the chains is exposed to air. Naturally, the ΔH_0 of a 2D crystal should be quite different from that of the bulk. The substrates, mica and sapphire, used in this study are attractive substrates for the it-PMMA. In order to keep the film in 2D, the attractive force between it-PMMA and the substrate should be stronger than the it-PMMA/it-PMMA interaction. Therefore, after melting the it-PMMA/it-PMMA interaction, strong interaction between the substrate and the it-PMMA should remain. Thus, the ΔH_0 may be reduced in the 2D crystal. On the other hand, the attractive interaction between the it-PMMA and the substrate may also reduce the ΔS_0 of melting, because after melting, the chain may retain some regularity on the substrate in comparison with a 3D crystal where a chain becomes a random coil. As a result, the attractive interaction of the substrate may reduce both ΔH_0 and ΔS_0 in the 2D crystal. However, the present result tends to indicate that the reduction of ΔS_0 is dominant compared to ΔH_0 , and as a result, T_m^0 should be increased in the 2D crystal, in order to explain the higher T_m observed here.

These very simple considerations indicate that we are far from understanding the properties of the 2D crystals, which may be very different from those of the bulk. Further theoretical development in our description of 2D crystals is needed to better understand their properties.

CONCLUSION

We evaluated the melting behavior of it-PMMA 2D crystals prepared by a LB technique using high-temperature AFM, and successfully observed the melting behavior *in situ* at high temperatures at the molecular level. The T_m of the 2D crystals was depressed significantly, by up to 90 °C. The T_m depression strongly depended on the molecular weight and also depended on the identity of the substrates. The large T_m depressions of the 2D crystals were not explained by a simple modified Thompson–Gibbs equation; theoretical improvements are necessary to understand the melting behavior of 2D crystal.

AUTHOR INFORMATION

Corresponding Author

*E-mail: kumaki@yz.yamagata-u.ac.jp

Present Address

[§]Yamagata Casio Co. Ltd., 5400-1, Higashine-ko, Higashine, Yamagata 999-3701, Japan.

Notes

The authors declare no competing financial interest.

ACKNOWLEDGMENTS

This work was supported by a Grant-in-Aid for Scientific Research on Innovative Areas “Molecular Soft-Interface Science” (20106009), Scientific Research (B) (21350059, 23360108, 24350113), and Challenging Exploratory Research (23655208, 24655091) from the Ministry of Education, Culture, Sports, Science, and Technology, Japan. We appreciate the assistance of Dr. Takehiro Kawauchi, Tokyo Institute of Technology, in the polymerization of the it-PMMA. We thank Professor Akihiro Nishioka, Keiji Katsuno, and Ryohei Uetake, Yamagata University, for their kind help with the DSC measurements. We also thank Assistant Professor Shotaro Nishitsuji, Yamagata University, for the WAXS measurements.

REFERENCES

- (1) Jones, R. L.; Kumar, S. K.; Ho, D. L.; Briber, R. M.; Russell, T. P. Chain Conformation in Ultrathin Polymer Films. *Nature* **1999**, *400*, 146–149.
- (2) Kraus, J.; Müller-Buschbaum, P.; Kuhlmann, T.; Schubert, D. W.; Stamm, M. Confinement Effects on the Chain Conformation in Thin Polymer Films. *Europhys. Lett.* **2000**, *49*, 210–216.
- (3) Hu, H. W.; Granick, S. Viscoelastic Dynamics of Confined Polymer Melts. *Science* **1992**, *258*, 1339–1342.
- (4) Zheng, X.; Sauer, B. B.; Van Alsten, J. G.; Schwartz, S. A.; Rafailovich, M. H.; Sokolov, J.; Rubinstein, M. Reptation Dynamics of a Polymer Melt near an Attractive Solid Interface. *Phys. Rev. Lett.* **1995**, *74*, 407–410.
- (5) Lin, E. K.; Wu, W.-L.; Satija, S. K. Polymer Interdiffusion Near an Attractive Solid Substrate. *Macromolecules* **1997**, *30*, 7224–7231.
- (6) O’Connell, P. A.; McKenna, G. B. Rheological Measurements of the Thermoviscoelastic Response of Ultrathin Polymer Films. *Science* **2005**, *307*, 1760–1763.
- (7) Keddie, J. L.; Jones, R. A. L.; Cory, R. A. Size-Dependent Depression of the Glass Transition Temperature in Polymer Films. *Europhys. Lett.* **1994**, *27*, 59–64.
- (8) Forrest, J. A.; Dalnoki-Veress, K.; Stevens, J. R.; Dutcher, J. R. Effect of Free Surfaces on the Glass Transition Temperature of Thin Polymer Films. *Phys. Rev. Lett.* **1996**, *77*, 2002–2005.
- (9) Fryer, D. S.; Peters, R. D.; Kim, E. J.; Tomaszewski, J. E.; de Pablo, J. J.; Nealey, P. F.; White, C. C.; Wu, W.-L. Dependence of the Glass Transition Temperature of Polymer Films on Interfacial Energy and Thickness. *Macromolecules* **2001**, *34*, 5627–5634.
- (10) Alcoutlabi, M.; McKenna, G. B. Effects of Confinement on Material Behaviour at the Nanometre Size Scale. *J. Phys.: Condens. Matter* **2005**, *17*, R461–R524.
- (11) Reiter, G.; Sommer, J.-U. Crystallization of Adsorbed Polymer Monolayers. *Phys. Rev. Lett.* **1998**, *80*, 3771–3774.
- (12) Taguchi, K.; Miyaji, H.; Izumi, K.; Hoshino, A.; Miyamoto, Y.; Kokawa, R. Growth Shape of Isotactic Polystyrene Crystals in Thin Films. *Polymer* **2001**, *42*, 7443–7447.
- (13) Wang, Y.; Ge, S.; Rafailovich, M.; Sokolov, J.; Zou, Y.; Ade, H.; Lüning, J.; Lustiger, A.; Maron, G. Crystallization in the Thin and Ultrathin Films of Poly(ethylene–vinyl acetate) and Linear Low-Density Polyethylene. *Macromolecules* **2004**, *37*, 3319–3327.
- (14) Wang, Y.; Rafailovich, M.; Sokolov, J.; Gersappe, D.; Araki, T.; Zou, Y.; Kilcoyne, A. D. L.; Ade, H.; Maron, G.; Lustiger, A. Substrate Effect on the Melting Temperature of Thin Polyethylene Films. *Phys. Rev. Lett.* **2006**, *96*, 028303.
- (15) Frank, C. W.; Rao, V.; Despotopoulou, M. M.; Pease, R. F. W.; Hinsberg, W. D.; Miller, R. D.; Rabolt, J. F. Structure in Thin and Ultrathin Spin-Cast Polymer Films. *Science* **1996**, *273*, 912–915.
- (16) Despotopoulou, M. M.; Frank, C. W.; Miller, R. D.; Rabolt, J. F. Kinetics of Chain Organization in Ultrathin Poly(*di-n*-hexylsilane) Films. *Macromolecules* **1996**, *29*, 5797–5804.
- (17) Despotopoulou, M. M.; Miller, R. D.; Rabolt, J. F.; Frank, C. W. Polymer Chain Organization and Orientation in Ultrathin Films: A Spectroscopic Investigation. *J. Polym. Sci., Part B: Polym. Phys.* **1996**, *34*, 2335–2349.
- (18) Schönherr, H.; Frank, C. W. Ultrathin Films of Poly(ethylene oxides) on Oxidized Silicon (2): In Situ Study of Crystallization and Melting by Hot Stage AFM. *Macromolecules* **2003**, *36*, 1199–1208.
- (19) Kim, J. H.; Jang, J.; Zin, W. C. Thickness Dependence of the Melting Temperature of Thin Polymer Films. *Macromol. Rapid Commun.* **2001**, *22*, 386–389.
- (20) Kumaki, J.; Kawauchi, T.; Yashima, E. Two-Dimensional Folded Chain Crystals of a Synthetic Polymer in a Langmuir–Blodgett Film. *J. Am. Chem. Soc.* **2005**, *127*, 5788–5789.
- (21) Kumaki, J.; Kawauchi, T.; Okoshi, K.; Kusanagi, H.; Yashima, E. Supramolecular Helical Structure of the Stereocomplex Composed of Complementary Isotactic and Syndiotactic Poly(methyl methacrylate)s as Revealed by Atomic Force Microscopy. *Angew. Chem., Int. Ed.* **2007**, *46*, 5348–5351.

- (22) Kumaki, J.; Kawauchi, T.; Ute, K.; Kitayama, T.; Yashima, E. Molecular Weight Recognition in the Multiple-Stranded Helix of a Synthetic Polymer without Specific Monomer–Monomer Interaction. *J. Am. Chem. Soc.* **2008**, *130*, 6373–6380.
- (23) Sakurai, S.-i.; Okoshi, K.; Kumaki, J.; Yashima, E. Two-Dimensional Hierarchical Self-Assembly of One-Handed Helical Polymers on Graphite. *Angew. Chem., Int. Ed.* **2006**, *45*, 1245–1248.
- (24) Sakurai, S.-i.; Okoshi, K.; Kumaki, J.; Yashima, E. Two-Dimensional Surface Chirality Control by Solvent-Induced Helicity Inversion of a Helical Polyacetylene on Graphite. *J. Am. Chem. Soc.* **2006**, *128*, 5650–5651.
- (25) Sakurai, S.-i.; Ohsawa, S.; Nagai, K.; Okoshi, K.; Kumaki, J.; Yashima, E. Two-Dimensional Helix-Bundle Formation of a Dynamic Helical Poly(phenylacetylene) with Achiral Pendant Groups on Graphite. *Angew. Chem., Int. Ed.* **2007**, *46*, 7605–7608.
- (26) Kajitani, T.; Okoshi, K.; Sakurai, S.-i.; Kumaki, J.; Yashima, E. Helix-Sense Controlled Polymerization of a Single Phenyl Isocyanide Enantiomer Leading to Diastereomeric Helical Polyisocyanides with Opposite Helix-Sense and Cholesteric Liquid Crystals with Opposite Twist-Sense. *J. Am. Chem. Soc.* **2006**, *128*, 708–709.
- (27) Onouchi, H.; Okoshi, K.; Kajitani, T.; Sakurai, S.-i.; Nagai, K.; Kumaki, J.; Onitsuka, K.; Yashima, E. Two- and Three-Dimensional Smectic Ordering of Single-Handed Helical Polymers. *J. Am. Chem. Soc.* **2008**, *130*, 229–236.
- (28) Maeda, T.; Furusho, Y.; Sakurai, S.-i.; Kumaki, J.; Okoshi, K.; Yashima, E. Double-Stranded Helical Polymers Consisting of Complementary Homopolymers. *J. Am. Chem. Soc.* **2008**, *130*, 7938–7945.
- (29) Ohsawa, S.; Sakurai, S.-i.; Nagai, K.; Banno, M.; Maeda, K.; Kumaki, J.; Yashima, E. Hierarchical Amplification of Macromolecular Heliicity of Dynamic Helical Poly(phenylacetylene)s Composed of Chiral and Achiral Phenylacetyles in Dilute Solution, Liquid Crystal, and Two-Dimensional Crystal. *J. Am. Chem. Soc.* **2011**, *133*, 108–114.
- (30) Sugihara, K.; Kumaki, J. Visualization of Two-Dimensional Single Chain Conformations Solubilized in Miscible Polymer Blend Monolayer by Atomic Force Microscopy. *J. Phys. Chem. B* **2012**, *116*, 6561–6568.
- (31) Kumaki, J.; Sakurai, S.-i.; Yashima, E. High-Resolution Atomic Force Microscopy of Synthetic Helical Polymers. *Chem. Soc. Rev.* **2009**, *38*, 737–746.
- (32) Mullin, N.; Hobbs, J. K. Direct Imaging of Polyethylene Films at Single-Chain Resolution with Torsional Tapping Atomic Force Microscopy. *Phys. Rev. Lett.* **2011**, *107*, 197801–1–5.
- (33) Pearce, R.; Vancso, G. J. Imaging of Melting and Crystallization of Poly(ethylene oxide) in Real-Time by Hot-Stage Atomic Force Microscopy. *Macromolecules* **1997**, *30*, 5843–5848.
- (34) Li, L.; Chan, C.-M.; Yeung, K. L.; Li, J.-X.; Ng, K.-M.; Lei, Y. Direct Observation of Growth of Lamellae and Spherulites of a Semicrystalline Polymer by AFM. *Macromolecules* **2001**, *34*, 316–325.
- (35) Hobbs, J. K.; Miles, M. J. Direct Observation of Polyethylene Shish-Kebab Crystallization Using in Situ Atomic Force Microscopy. *Macromolecules* **2001**, *34*, 353–355.
- (36) Hobbs, J. K.; Humphris, A. D. L.; Miles, M. J. In Situ Atomic Force Microscopy of Polyethylene Crystallization. 1. Crystallization from an Oriented Backbone. *Macromolecules* **2001**, *34*, 5508–5519.
- (37) Ivanov, D. A.; Amalou, Z.; Magonov, S. N. Real-Time Evolution of the Lamellar Organization of Poly(ethylene terephthalate) during Crystallization from the Melt: High-Temperature Atomic Force Microscopy Study. *Macromolecules* **2001**, *34*, 8944–8952.
- (38) Beekmans, L. G. M.; van der Meer, D. W.; Vancso, G. J. Crystal Melting and Its Kinetics on Poly(ethylene oxide) by in Situ Atomic Force Microscopy. *Polymer* **2002**, *43*, 1887–1895.
- (39) Magonov, S. N.; Yerina, N. A.; Ungar, G.; Reneker, D. H.; Ivanov, D. A. Chain Unfolding in Single Crystals of Ultralong Alkane $C_{390}H_{782}$ and Polyethylene: An Atomic Force Microscopy Study. *Macromolecules* **2003**, *36*, 5637–5649.
- (40) Xu, J.; Guo, B.-H.; Zhang, Z.-M.; Zhou, J.-J.; Jiang, Y.; Yan, S.; Li, L.; Wu, Q.; Chen, G.-Q.; Schultz, J. M. Direct AFM Observation of Crystal Twisting and Organization in Banded Spherulites of Chiral Poly(3-hydroxybutyrate-*co*-3-hydroxyhexanoate). *Macromolecules* **2004**, *37*, 4118–4123.
- (41) Wang, Y.; Chan, C.-M.; Ng, K.-M.; Jiang, Y.; Li, L. Real-Time Observation of Lamellar Branching Induced by an AFM Tip and the Stability of Induced Nuclei. *Langmuir* **2004**, *20*, 8220–8224.
- (42) Hobbs, J. K.; Farrance, O. E.; Kailas, L. How Atomic Force Microscopy Has Contributed to Our Understanding of Polymer Crystallization. *Polymer* **2009**, *50*, 4281–4292.
- (43) Hatada, K.; Ute, K.; Tanaka, K.; Okamoto, Y.; Kitayama, T. Living and Highly Isotactic Polymerization of Methyl Methacrylate by *tert*-C₄H₉MgBr in Toluene. *Polym. J.* **1986**, *18*, 1037–1047.
- (44) Yoshimoto, M.; Maeda, T.; Ohnishi, T.; Koinuma, H.; Ishiyama, O.; Shinohara, M.; Kubo, M.; Miura, R.; Miyamoto, A. Atomic-Scale Formation of Ultrasmooth Surfaces on Sapphire Substrates for High-Quality Thin-Film Fabrication. *Appl. Phys. Lett.* **1995**, *67*, 2615–2617.
- (45) Kusy, R. P. Determination of the Heat of Fusion of Isotactic Poly(methyl methacrylate). *J. Polym. Sci., Polym. Chem. Ed.* **1976**, *14*, 1527–1536.
- (46) Owens, D. K.; Wendt, R. C. Estimation of the Surface Free Energy of Polymers. *J. Appl. Polym. Sci.* **1969**, *13*, 1741–1747.
- (47) Kwok, D. Y.; Neumann, A. W. Contact Angle Measurement and Contact Angle Interpretation. *Adv. Colloid Interface Sci.* **1999**, *81*, 167–249.
- (48) Schultz, J.; Tsutsumi, K.; Donnet, J.-B. Surface Properties of High-Energy Solids: I. Determination of the Dispersive Component of the Surface Free Energy of Mica and Its Energy of Adhesion to Water and *n*-Alkanes. *J. Colloid Interface Sci.* **1977**, *59*, 272–276.
- (49) Schultz, J.; Tsutsumi, K.; Donnet, J.-B. Surface Properties of High-Energy Solids: II. Determination of the Nondispersing Component of the Surface Free Energy of Mica and Its Energy of Adhesion to Polar Liquids. *J. Colloid Interface Sci.* **1977**, *59*, 277–282.
- (50) Brinkhuis, R. H. G.; Schouten, A. J. Thin-film Behavior of Poly(methyl methacrylates). 1. Monolayers at the Air–Water Interface. *Macromolecules* **1991**, *24*, 1487–1495.
- (51) Kusanagi, H.; Tadokoro, H.; Chatani, Y. Double Strand Helix of Isotactic Poly(methyl methacrylate). *Macromolecules* **1976**, *9*, 531–532.
- (52) Kusanagi, H.; Chatani, Y.; Tadokoro, H. The Crystal Structure of Isotactic Poly(methyl methacrylate): Packing-Mode of Double Stranded Helices. *Polymer* **1994**, *35*, 2028–2039.